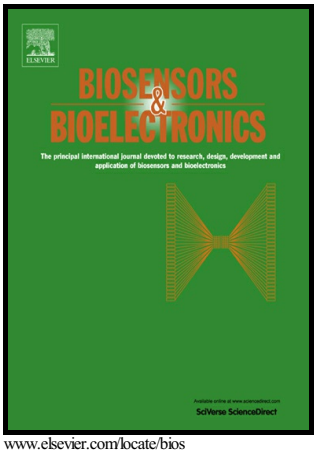

www.elsevier.com/locate/bios

A multidimensional design of charge transfer interfaces via D–A–D linking fashion for electrophysiological sensing of neurotransmitters

He Liu, Chaoyi Liu, Yue Gu, Cong Li, Xiaoyi Yan, Tingting Zhang, Nannan Lu, Bo Zheng, Yaru Li, Zhiquan Zhang, Ming Yang

PII: S0956-5663(17)30516-X
DOI: http://dx.doi.org/10.1016/j.bios.2017.07.058
Reference: BIOS9891

To appear in: *Biosensors and Bioelectronic*

Received date: 12 April 2017
Revised date: 13 July 2017
Accepted date: 24 July 2017

Cite this article as: He Liu, Chaoyi Liu, Yue Gu, Cong Li, Xiaoyi Yan, Tingting Zhang, Nannan Lu, Bo Zheng, Yaru Li, Zhiquan Zhang and Ming Yang, A multidimensional design of charge transfer interfaces via D–A–D linking fashion for electrophysiological sensing of neurotransmitters, *Biosensors and Bioelectronic,* http://dx.doi.org/10.1016/j.bios.2017.07.058

A multidimensional design of charge transfer interfaces via D–A–D linking fashion for electrophysiological sensing of neurotransmitters

He Liu[a], Chaoyi Liu[b], Yue Gu[a], Cong Li[a], Xiaoyi Yan[a], Tingting Zhang[a], Nannan Lu[a], Bo Zheng[a], Yaru Li[a], Zhiquan Zhang[a]*, Ming Yang[c]*

[a] *College of Chemistry, Jilin University, Changchun 130012, China*

[b] *State Key Laboratory of Supramolecular Structure and Materials, College of Chemistry, Jilin University, Changchun 130012, China*

[c] *Department of Breast Surgery, First Hospital, Jilin University, Changchun 130012, PR China*

[*] Corresponding author. Tel: +86-431-85168352-7; Fax: +86-431-85168399

E-mail address: zzq@jlu.edu.cn (Z. Zhang); yangming1967@163.com (M. Yang)

Abstract:

Donor–Acceptor (D–A) structure like host-guest pair serves as an organic charge–transfer (C–T) material with pregnant electrochemical and photochemical properties. Phenothiazine, a conjugated nitrogen-sulfur heterocyclic compound with broad pharmaceutical profile, is a strong electron donating system and applied in the synthesis of various classic antipsychotic drugs. In this proposal, a novel D–A molecule, 2,3-bis(4-(10H-phenothiazin-10-yl)phenyl)fumaronitrile (PTBFN), containig a diphenylfumaronitrile as the electrophilic central core and two phenothiazines as the peripheral electron donor functional groups is first designed and synthesized. Subsequently, the C–T layer based on the PTBFN polymer, poly(PTBFN), is obtained via a straightforward electrochemical method and used as an efficient electrocatalyst for dopamine (DA) detection. The logarithm of oxidation peak currents present an outstanding linear response to that of the DA concentration varying from 0.005 to 350 μM with a detection limit down to 0.70 nM, wherein the interferences of uric acid (UA) and ascorbic acid (AA) could be eliminated effectively. Moreover, the biosensor displays decent stability, excellent selectivity for different interfering compounds and applicability in real samples analysis. The favorable sensing performance suggests that the nontrivial D–A architecture is one of the promising bioaffinity catalysts for electrocatalysis and expected to provide wider application potential for biosensing construction and medical diagnostics.

Keywords: Donor–Acceptor (D–A) structure, Bioaffinity sensor, Charge–transfer,

Phenothiazine, Dopamine.

1. Introduction

Dopamine (DA), as a neurotransmitter within the brain, is responsible for the regulation of central nervous, hormonal, cardiovascular as well as renal systems (Heien et al., 2005). Several disorders of the nervous system such as Parkinson's disease (Hirsch et al., 1988), schizophrenia (Grace, 2012) and attention deficit hyperactivity disorder (Wightman et al., 1988) are due to extremely abnormal concentration of DA. Consequently, accurate determination of DA would further a better understanding of these pathophysiological effects and could develop a tool to carry out the output of the treatments. The most elegant techniques for DA determination are high performance liquid chromatography (Park et al., 2013), fluorescence methods (Lu et al., 2011), surface-enhanced Raman scattering (An et al., 2015), colorimetric visualization (Kong et al., 2011). As compared to other analytical methods, electrochemical sensing is an advantageous way for the detection in vivo and in vitro owing to rapid detection, excellent sensitivity, high selectivity, low cost and ease of operation (Cao et al., 2004; Feng et al., 2017; Guohua et al., 2017; Hu et al., 2017; Hui et al., 2016; Li et al., 2016; Liu et al., 2017; Qin et al., 2016; Zhang et al., 2017; Zhang et al., 2016; Zhou et al., 2016; Zou et al., 2017). Nonetheless, considering the low concentration of DA (0.01–1 μM) and the interferences from both electroactive uric acid (UA) and ascorbic acid (AA) in the extracellular fluid, it remains a substantial challenge for quantitative analysis of DA. To surmount these

difficulties, various materials have been established such as 2D hexagonal boron nitride (Khan et al., 2016), thiazole-based copolymer (Zhang et al., 2013b) and nanostructured nickel oxide (Roychoudhury et al., 2015) to accurately estimate DA. Progress is being made, the novel material we envisaged is expected to significantly improve sensitivity and selectivity of DA detections.

Conducting polymer film manufactured by electropolymerization of pyrrole, aniline, carbazole, thiophene, and their derivatives, as the flexible electrode materials, have attracted considerable research interest in virtue of their natural characteristics (*e.g.* high electrical conductivity and intriguing redox properties) (Bredas et al., 2002; Chauhan et al., 2017; Cosnier et al., 2003; Mao et al., 2015; Wang et al., 2017). And molecular wire theory is an appealing alternative. Swager et al. demonstrates that the conjugated polymers are interconnecting as a molecular wire and superior over other materials (small molecular-based and inorganic semiconductors) due to their robust conductivity of the backbone in measurable system (Zhang et al., 2013a). Recently, promising emerging materials with donor–acceptor (D–A) architecture have improved the performance of charge–transfer (C–T), conductivity and exciton migration, compared to their parent conjugated polymers (Ullah et al., 2017). In view of these facts, we have reasoned that D–A conjugated polymers can form a new platform for the signal-enhancing by mediating a fast electron transfer between the analyte and an electrode system. D–A structure capable of ambipolar charge (electron and hole) has been explored as C–T materials in organic light-emitting diode (Kraft et al., 1998),

electrochromism (Lv et al., 2017), photovoltaic cells (Sonmez et al., 2005) and organic thin film transistors (Champion et al., 2010). However, its applications in electrochemical sensors are less reported (Kumar et al., 2014).

Inspired by the success in constructing appropriate D and A building blocks, phenothiazine unit has drawn our attention, owing to it possesses the π-delocalization in the central ring cation radical. Some studies have reported that phenothiazine had a fused tricyclic structure similar to that of carbazole, was a stronger and potentially better electron donor than the carbazole unit due to its 0.7 eV lower ionization potential (Kulkarni et al., 2010; Kulkarni et al., 2005; Yao et al., 2014). In addition, a three-carbon chain among the nitrogen atom of the phenothiazine core and the terminal nitrogen of the side chain is the pivotal feature in relation to psychotropic activity (Sudeshna and Parimal, 2010). The phenothiazine group of drugs are used for clinical treatment of psychosis for more than sixty years and primarily to regulate the dynamics of fluctuating DA concentrations (Ohlow and Moosmann, 2011). Because of these characteristics, the functionalized phenothiazine-based molecules, which have been employed as potent pharmacophoric section in pharmacology and biomedicine (Pluta et al., 2011a), may be served as novel electrocatalysts for electrochemical detection of DA. Firstly, the non-planar phenothiazine ring conformation hinders π-stacking aggregation in the polymer main-chains or interaction among analytes, creating a biomimetic microenvironment for the electrochemical recognition process (XX et al., 2003). Secondly, the strong

electron-donating property of phenothiazine gives the polymer a low oxidation potential and an enhanced electrocatalytic activity (Jo et al., 2014). Thirdly, the unique biological activities of phenothiazines on biological systems may be able to exhibit high affinity molecular recognition for DA (Mocko et al., 2010; Pluta et al., 2011b). Diphenylfumaronitrile unit displays distinct advantages as acceptor building block for constructing C–T materials with its two cyano functionalities (Shen et al., 2013). It can provide an extended π-conjugated system and effectively reduce the bandgap. Katz and co-workers also used diphenylfumaronitrile building block to achieve an electron mobility of 0.027 $cm^2 V^{-1} s^{-1}$ for vacuum deposited thin film (Lee et al., 2009).

As a proof of concept, 2,3-bis(4-(10H-phenothiazin-10-yl)phenyl)fumaronitrile (PTBFN), a novel π-conjugated D–A compound bestows PTBFN with enhanced intramolecular C–T property, has been first designed to provide great electron delocalization all over the conjugated branches through the whole molecule. And then its conjugated oligomer is gained after a facile electrochemical method. When the electronic and biocompatible properties investigated by our previous studies for selective donor and acceptor units extrapolate to conjugated oligomers with D–A–D linking fashion, two main functions exquisitely influence the analytical performance for DA, namely: (1) The introduced D–A based biosensor is a signal-enhancing system, which relies on amplification by the collective minor current change and acceleration by energy transfer between the DA and electrode surface. (2) An

ingenious design of phenothiazine donor, which has maintained non-planar phenothiazine ring, can be as a biorecognition element for specific detection of DA against AA, UA and other analogous endogenous compounds. All above factors endow the biosensor with completely new performance and characteristics.

2. Experimental

2.1. Reagents and apparatus

This section can be found in the Supplementary material.

2.2. Synthesis of the PTBFN monomer

The prepared route of PTBFN was elucidated by Scheme. S1 (Supporting Information). PTBFN was synthesized according to a Suzuki coupling reaction between corresponding phenothiazine and 2,3-bis(4-bromophenyl)fumaronitrile. The starting compound 2,3-bis(4-bromophenyl)fumaronitrile (A) was prepared by reacting 4-bromophenylacetonitrile according to the previous reports (Yeh et al., 2003). The mixture of A (3.0 mmol), phenothiazine (6.6 mmol), sodium tert-butoxide (3.6 mmol), toluene (40 mL), tri-tert-butylphosphine tetrafluoroborate (0.142 g) were dissolved and degassed before $Pd_2(dba)_3$ (0.0474 g) was added under nitrogen. The resulting solution was stirred for 48 h at 110°C and cooled to room temperature. It was then poured into 50ml water to the reaction mixture and the product was extracted with CH_2Cl_2 for three times. Removal of the solvent afforded the crude product, which was further purified using column chromatography on silica gel (a mixture of petroleum ether/CH_2Cl_2=3:1 as eluent) to give the product as a bright red solid (yield 20%).

2.3. Sensor fabrication

Prior to modification, the bare GCE was polished successively in 1.0, 0.3 and 0.05 μm alumina slurries on microcloth pads. Then, it was sonicated successively in 1:1 nitric acid, ethanol and water, each for 1 min, and dried under a stream of nitrogen. The electrode surface derivatization was carried out in N,N-dimethylformamide/acetonitrile = 3:2 (v/v) solution containing 1.000 mg mL^{-1} PTBFN and 100.0 mM lithium perchlorate as a supporting electrolyte through consecutive cyclic voltammetry by scanning the potential from –1.2 V to 2.0 V (versus Ag wire) at 0.1 V s^{-1} for 15 cycles. The electrode was then removed and washed with large volumes of acetonitrile.

3. Results and discussions

3.1. Electropolymerization of PTBFN

The mechanism for the electropolymerization of PTBFN and corresponding control experiments are described in the Supplementary material.

3.2. Characterizations of PTBFN monomer and poly(PTBFN) film

Fig. S5 offers ^{1}H NMR spectrum of PTBFN. ^{1}H NMR (500 MHz, DMSO): δ = 7.90 (d, J = 8.6 Hz, 4H), 7.42 (d, J = 7.7 Hz, 4H), 7.35 (d, J = 8.7 Hz, 4H), 7.31-7.25 (m, J = 7.7 Hz, 4H), 7.20-7.14 (m, J = 7.5 Hz, 4H), 7.04 (d, J = 8.0 Hz, 4H).

As observed in Fig. 1a, most of the IR frequencies in the spectra of polymer are close to those of its parent monomer with only a little indication of changing of aromatic ring substituents in the range of 900 to 700 cm^{-1} (Schlereth and Karyakin,

1995). The absorption band for the monomer at 1611 cm^{-1} attributed to the C=C stretching vibration of aromatic ring and that at 1382 cm^{-1} corresponding to the tertiary amino group stretching vibration shift to 1621 cm^{-1} and 1384 cm^{-1} in the IR spectra of its derived polymer, respectively (Xiao et al., 2011). The spectra of PTBFN and poly(PTBFN) also have similar signals at 2341 cm^{-1} and 2348 cm^{-1} due to the C≡N stretching vibration. The signals at 1115 cm^{-1} and 1089 cm^{-1} are assigned to vibrations of the C–S, which remains unchanged in the monomer and polymer. The peaks at 861 and 770 cm^{-1} do not appear in the FT-IR spectrum of poly(PTBFN), indicating the polymerization happened. The characteristic peaks of poly(PTBFN) at ~885, ~805 cm^{-1} indicate the presence of 1,2,4-trisubstitution of benzene ring in the polymerization process. Therefore, the mechanism of polymerization of PTBFN deduced from the IR profile is agreement with our previous analysis.

In UV-vis absorption spectra, PTBFN monomer and its polymer film exhibit very distinct spectral properties, which manifest that conjugated polymers are formed upon electropolymerization. As shown in Fig. 1b, the monomer has prominent peaks at about 235 nm and 324 nm. After polymerization, the absorption peak at 235 nm dramatically decreases accompanying by a 26 nm red shift and the absorption feature at 324 nm converts to a hump. The significant red shift and a new peak at 440 nm may be related to strengthen the conjugated system in poly(PTBFN) main chain. Furthermore, the disappeared absorption peak at about 324 nm is presumably attributed to electrochemical formation of the cation-radicals in phenoxazine rings and

the relatively higher asymmetrical dimers of poly(PTBFN).

The zoomed-in SEM image shows a nano-/microwire-like poly(PTBFN) structure, which is similar to the molecular wire theory as forementioned. Fig. 1c displays a squamous stratified texture of the linear polymer, where more functionalized edge sites would be exposed to the analyte. The three-dimensional film structure explains the steric effects of the oligomer growth. Thus, electropolymerization of PTBFN has the potential to provide larger accessible surface area and higher electrocatalytic efficiency.

3.3. Electrochemical impedance spectroscopy (EIS) analysis

The C–T resistance (R_{ct}) of electrode surface is probed by EIS in the presence of electrolyte (0.1 M KCl solution including 10 mM $[Fe(CN)_6]^{3-/4-}$). The bare GCE and the poly(PTBFN)/GCE present semicircle portions and linear portions, as in Fig. 1d. A typical complex plane of a faradic impedance spectra consists of a semicircle part at higher frequencies corresponding to a C–T limited process and a straight-line part at lower frequencies corresponding to a diffusion limited process. The R_{ct} equates the semicircle diameter in the spectra and can be analysed by fitting the EIS results using the equivalent circuit (inset of Fig. 1d) (Guo et al., 2012). Hence, we can infer impedance changes of the modified electrode by calculating the diameter of semicircles in the plot. As expected, the diameter of the GCE deposited with poly(PTBFN) (R_{ct} = 108.7 Ω) is obviously smaller than that of bare GCE (R_{ct} = 267.5 Ω). The decrease of impedance value is attributed to easier conduction of

$[Fe(CN)_6]^{3-/4-}$ redox reaction, indicating that the electroactive polymer can accelerate electron transport and diminish the energy barriers of the heterogeneous reaction.

< Fig. 1 >

3.4. Electrocatalytical oxidation of DA at biosensor

After characterisation of the polymer film, the electrochemical responses of DA at the bare GCE and the poly(PTBFN)/GCE are measured using cyclic voltammetry (CV) in a 300 μM DA solution. As shown in Fig. 2a, there is a pair of relatively weak redox peaks with low peak currents and high peak-to-peak separation (ΔE_p = 257 mV) at the bare GCE(A), suggesting that the bare GCE is failed to determine lower concentration of DA. In contrast, at the poly(PTBFN)/GCE(B), the peak currents remarkably increase by a factor of 6.5 and the ΔE_p value decreases to 70 mV, which mean that poly(PTBFN) is an excellent conductive film. The enhanced electrochemical sensing properties observed at the polymer-modified biosensor can be principally ascribed to the following major factors: (1) Electrochemical recognition: the hydrogen atoms of DA interact with the nitrogen atoms of poly(PTBFN) chain, which can boost a faster dehydrogenation rate in the DA oxidation and accelerate the kinetics of the whole reaction. Meanwhile, not compact but squamous stratified structure of the poly(PTBFN) possesses a more active area, providing a biomimetic microenvironment for the oxidation of DA. (2) Electrocatalysis: the robust electron-donating inherent quality of phenothiazine gives the PTBFN molecular a low ionization potential and easily forms cationic polymer film, exhibiting the favorable

interaction with DA at a less-positive potential. (3) Signal amplification: benefiting from the conducting abilities of D–A structure, poly(PTBFN) as a redox mediator induces an efficient energy migration with the extension of conjugated backbone, accordingly, the measurable signal system is easily perturbed by external agents and then offers a noteworthy current change. Chronocoulometry is also used to provide electrochemical evidence to the characterize the oxidation of DA and the relevant details can be found in the Supplementary material. The schematic illustration about the fabrication process of sensor and DA electrocatalytic oxidation is depicted in Scheme. 1.

< Scheme. 1 >

3.5. Catalytic kinetic analysis

As we are encouraged by the beneficial potential toward DA oxidation and ΔE_p = 70 mV, we go further to verify the prominent electrocatalytic process by chronoamperometry (Fig. 2b). The catalytic rate constant between DA and poly(PTBFN)/GCE can be evaluated according to following equation (Harrison and Khan, 1970):

$$I_C/I_L = \pi^{1/2}(k_cCt)^{1/2} \quad (1)$$

where I_C is the catalytic current and I_L is the limited current in the presence and absence of DA at the elapsed time t, respectively. The value of k_c ($1.99 \times 10^4\ M^{-1}\ s^{-1}$) can be calculated for a given bulk concentration of DA, which is higher than that previous reported (Hsieh and Whang, 2017), confirming that the conducting layer of

poly(PTBFN) endows high catalytic activity in the process of DA electrocatalytical oxidation.

< Fig. 2 >

3.6. Optimization of detection conditions

3.6.1. Effect of solution pH

The pH values of the buffer solution have a significant influence on the oxidation of DA, by varying both the peak currents and peak potentials. In the pH range from 3.0 to 9.0, it is observed that the redox peak potentials shift negatively with the increase of pH (Fig. 3a). The result indicates that protons are related to the electrode reaction. According to the linear regression equation for DA E_{pa} (mV) = −66.39 pH + 653.8 (R = 0.997), the slope is close to the Nernstian value of 59 mV/pH at 25°C, which represents an equal number of electron and proton transfer process. Inset of Fig. 3b reveals that the largest peak current is obtained at pH 6.0, and this value is chosen as the optimum pH for the detection of DA to achieve high sensitivity.

< Fig. 3 >

3.6.2. Effect of scan rate

CV curves with different scanning rates are explored to determine that the DA oxidation is controlled by diffusion or adsorption processes on the biosensor (Fig. 4a). Fig. 4b demonstrates the linear dependence of both anodic and cathodic currents against the square root of scan rate with the linear equation of I_{pa} (μA) = 1.9007 $\nu^{1/2}$ (mV s^{-1})$^{1/2}$ − 1.4923 (R^2 = 0.9978). This result indicates that the redox process at the

poly(PTBFN)/GCE is controlled by diffusion. The following equation can be used to calculate the diffusion coefficient of DA:

$$I_p = 2.69 \times 10^5 [\text{A s mol}^{-1}\ \text{V}^{-1/2}] A n^{3/2} D_0^{1/2} C_0 \text{V}^{1/2} \quad (2)$$

where n means the electron involved in the overall catalytic reaction, A means the active area of electrode (0.219 cm^2), which is measured by chronoamperometry in 1 mM $K_3[Fe(CN)_6]$ solution containing 0.1 M KCl using the Cottrell equation (Bard and Faulkner, 1980), C_0 means the bulk concentration of the analyte, D_0 means the diffusion coefficient of DA and is calculated as 6.2×10^{-6} cm^2 s^{-1} with other known parameters and constants. This result agrees consistently with the reported ones (Yan et al., 2016).

< Fig. 4 >

3.7. Rotating disk electrode (RDE) voltammetry

The more kinetics informations of DA oxidation at poly(PTBFN) modified GCE are generated using a rotating disk electrode (RDE). Typical examples of the *I–E* curves (RDE voltammograms) show that the catalyzed currents are limited by various rotation rates from 200 to 5000 rpm (Fig. S6). The limiting currents remain proportional to the square root of the rotation rate, signifying that the polarization curves are controlled by mass-transport. This occurrence should obey the Koutecky-Levich equation (Oyama and Anson, 2002):

$$I_{Lev} = 0.62 n c F A D^{2/3} u^{-1/6} \omega^{1/2} \quad (3)$$

where, I_{Lev}, F, and A are Levich current, Faraday constant (96,485.3 C mol^{-1}),

electrochemical active electrode area, respectively, D (6.2×10^{-6} cm^2 s^{-1}) represents diffusion coefficient calculated from former section, u (0.01 cm^2 s^{-1}) represents the kinematic viscosity of medium, ω (rad s^{-1}) represents rotation speed. The outcome of n represents the transferred electron number and is calculated to be 2.111 ≈ 2, suggesting that DA is oxidized by exchanging 2 electrons and 2 protons.

3.8. Calibration curve

Differential pulse voltammetry (DPV) has a much higher current sensitivity and lower background compared with CV. The DPV curves for different concentration of DA on poly(PTBFN)/GCE are recorded in Fig. 5a, where upon addition of DA, an increase in the current relating to the oxidation peak of DA at 0.18 V is observed in the range 0.005–350 μM. Owing to high electroactivity, DA easily gets oxidized resulting the formation of dopamine quinone by exchanging 2 electrons and 2 protons. The linear regression equation is got as $\log I_{pa}$ (nA) = 0.6165 log$C$ (nM) + 1.2431 (R = 0.9986). The detection limit is determined to be 0.70 nM with a relative standard deviation of 1.0 % (n=5) by the relation 3s/m, where s is the standard deviation of the blank peak currents and m is the slope of the calibration curve. Table.S1 and Table.S2 summarizes the analytical parameters of different modified electrodes and techniques for the detection of DA, respectively. Among these various reports, the multifunctional redox mediator of poly(PTBFN) is a preferable electrocatalyst for DA oxidation. Such a high degree of D–A conjugated polymer induces an efficient energy migration with the extension of conjugated backbone, accordingly, the measurable

signal system is easily perturbed by external agents and then offered a noteworthy current change.

< Fig. 5 >

3.9. Interferences, reproducibility and stability

An effective biosensor requires not just the sensitivity of the signal transducer but also selectivity of the molecular recognition. To study the effect of interferences by possible co-existing compounds and evaluate the validity of the detection, we find that 10 fold concentration of K^+, Na^+, Li^+, Ca^{2+}, Cl^-, NO_3^-, ClO_4^-, SO_4^{2-}, HPO_4^{2-}, 3 fold concentration of glucose, UA, AA have a neglected response to the current change, which exhibites satisfying selectivity for DA, and justifies the affinity of phenothiazine-based compound and DA (Fig. S7). More details about negative control experiments can be found in the Supplementary material. Reproducibility of poly(PTBFN)/GCE in the measurements is evaluated by detection of DA for the ten successive use of the same electrode and the relative standard deviation (RSD) of less than 5%. After storing the poly(PTBFN)/GCE for 30 days, only a small decrease of the anodic peak current is obtained, with a signal change of 3.16% for DA (Fig. S8). These desirable levels of reproducibility and stability confirm that the polymeric sensing film is very stable and seldom leached out of the GCE surface.

3.10. Application of the biosensor in real samples

The practical analytical utility of the proposed biosensor is assessed by detecting the concentration of DA in human serum, human urine and lake water. These real

samples are diluted 60-times with PBS solution (pH 6.0). The detailed experimental data are listed in Table S3 with the recovery in the range of 96.4–104.3 % and the RSD value less than 4.0 %, revealing the reliability for DA determination in real samples.

4. Conclusions

In summary, the D–A compound of PTBFN, is rationally designed and synthesized according to a Suzuki coupling reaction using phenothiazine as the donor and diphenylfumaronitrile as the acceptor. As a result, the novel biosensor exhibits a wider linearity (0.005–350 μM), a lower limit of detection (0.7 nM), and a higher catalytic rate data (1.99×10^4 M^{-1} s^{-1}) with longer stability toward DA detection. It is suggested that, the poly(PTBFN) functionalized GCE sensing platform opens up a new DA detection model, without using extra-biomolecule auxiliary, just by minimalism ideas of electropolymerized conductive film for ultrasensitive detection. Even more importantly, our work can also be easily extended to other types of D–A conducting polymers to investigate the effects of their morphologies and electronic structures on relevant electrophysiological sensing performance. Our investigation along this way is in progress.

Acknowledgements

This work was supported by the National Natural Science Foundation of China (No. 21375045) and Natural Science Foundation of Jilin Province (No.

20130101118JC).

Reference

An, J.H., Choi, D.K., Lee, K.J., Choi, J.W., 2015. Biosens. Bioelectron. 67, 739-746.

Bard, A.J., Faulkner, L.R., 1980. Electrochemical methods : fundamentals and applications. Wiley.

Bredas, J.L., Silbey, R., Boudreaux, D.S., Chance, R.R., 2002. J. Am. Chem. Soc. 105, 6555-6559.

Cao, Y., Wang, Y., Chen, X., Ye, J., 2004. Food Chem. 86, 131-136.

Champion, R.D., Cheng, K.F., Chia‐Ling, P., Chen, W.C., Jenekhe, S.A., 2010. Macromol. Rapid. Comm. 26, 1835-1840.

Chauhan, N., Chawla, S., Pundir, C.S., Jain, U., 2017. Biosens. Bioelectron. 89, 377-383.

Cosnier, S., Pellec, A.L., Marks, R.S., Périé, K., Lellouche, J.P., 2003. Electrochem. Commun. 5, 973-977.

Feng, H., Huang, Z., Lou, X., Li, J., Hui, G., 2017. Food Analytical Methods 10, 407-418.

Grace, A.A., 2012. Neuropharmacology 62, 1342.

Guo, X., Kulkarni, A., Doepke, A., Halsall, H.B., Iyer, S., Heineman, W.R., 2012. Anal. Chem. 84, 241.

Guohua, H., Hongyang, L., Zhiming, J., Danhua, Z., Haifang, W., 2017. Biosens. Bioelectron. 97, 184-195.

Harrison, J.A., Khan, Z.A., 1970. J. Electroanal. Chem. 28, 131-138.

Heien, M.L., Khan, A.S., Ariansen, J.L., Cheer, J.F., Phillips, P.E., Wassum, K.M., Wightman, R.M., 2005. P. Acad. Nat. Sci. 102, 10023-10028.

Hirsch, E., Graybiel, A.M., Agid, Y.A., 1988. Nature 334, 345.

Hsieh, M.-T., Whang, T.-J., 2017. Appl. Surf. Sci. 396, 1589-1595.

Hu, L., Zou, L., Qin, Z., Fang, J., Huang, L., Wang, P., 2017. Sensors and Actuators B: Chemical 238, 1151-1158.

Hui, G., Zhang, J., Li, J., Zheng, L., 2016. Food Chem. 197 Pt B, 1168-1176.

Jo, H.J., Nam, J.E., Kim, D.H., Kim, H., Kang, J.K., 2014. Dyes. Pigments. 102, 285-292.

Khan, A.F., Brownson, D.A.C., Randviir, E.P., Smith, G.C., Banks, C.E., 2016. Anal. Chem. 88.

Kong, B., Zhu, A., Luo, Y., Tian, Y., Yu, Y., Shi, G., 2011. Angew. Makromol. Chem. 50, 1837.

Kraft, A., Grimsdale, A.C., Holmes, A.B., 1998. Cheminform 29, no-no.

Kulkarni, A.P., Kong, X., Jenekhe, S.A., 2010. Adv. Funct. Mater. 16, 1057-1066.

Kulkarni, A.P., Wu, P.-T., Kwon, T.W., Jenekhe, S.A., 2005. J. Phys. Chem. B 109, 19584-19594.

Kumar, P., Saravanan, S., Ranjith, K., Ramamurthy, P.C., 2014. J. Appl. Electrochem. 44, 133-139.

Lee, T., Landis, C.A., Dhar, B.M., Jung, B.J., Sun, J., Sarjeant, A., Lee, H.J., Katz, H.E., 2009. J. Am. Chem. Soc. 131, 1692.

Li, J., Feng, H., Liu, W., Gao, Y., Hui, G., 2016. Food Analytical Methods 9, 2943-2951.

Liu, L., Zhang, D., Zhang, Q., Chen, X., Xu, G., Lu, Y., Liu, Q., 2017. Biosens. Bioelectron. 93, 94-101.

Lu, L.M., Zhang, X.B., Kong, R.M., Yang, B., Tan, W., 2011. J Am Chem Soc. 133, 11686-11691.

Lv, X., Li, W., Ouyang, M., Zhang, Y., Wright, D.S., Zhang, C., 2017. J. Mater. Chem.C 5, 12-28.

Mao, H., Liang, J., Zhang, H., Qi, P., Liu, D., Wu, S., Zhang, Y., Song, X.M., 2015. Biosens. Bioelectron. 70, 289-298.

Mocko, J.B., Kern, A., Moosmann, B., Behl, C., Hajieva, P., 2010. Neurobiol. Dis. 40, 120.

Ohlow, M.J., Moosmann, B., 2011. Drug Discov. Today 16, 119-131.

Oyama, N., Anson, F.C., 2002. Anal. Chem. 52, 1192-1198.

Park, J.Y., Myung, S.W., Kim, I.S., Choi, D.K., Kwon, S.J., Yoon, S.H., 2013. Biol. Pharm. Bull. 36, 252-258.

Pluta, K., Morak-Młodawska, B., Jeleń, M., 2011a. Eur. J. Med. Chem. 46, 3179.

Pluta, K., Morak-Młodawska, B., Jeleń, M., 2011b. Eur. J. Med. Chem. 46, 3179-3189.

Qin, Z., Zhang, B., Hu, L., Zhuang, L., Hu, N., Wang, P., 2016. Biosens. Bioelectron. 78, 374-380.

Roychoudhury, A., Basu, S., Jha, S.K., 2015. Biosens. Bioelectron. 84, 72-81.

Schlereth, D.D., Karyakin, A.A., 1995. J. Electroanal. Chem. 395, 221-232.

Shen, X.Y., Wang, Y.J., Zhao, E., Yuan, W.Z., Liu, Y., Lu, P., Qin, A., Ma, Y., Sun, J.Z., Tang, B.Z., 2013. J. Phys. Chem. C 117, 7334-7347.

Sonmez, G., Shen, C.K.F., Rubin, Y., Wudl, F., 2005. Adv. Mater. 17, 897-900.

Sudeshna, G., Parimal, K., 2010. Eur. J. Pharmacol. 648, 6-14.

Ullah, H., Bibi, S., Tahir, A.A., Mallick, T.K., 2017. J. Alloy. Compd. 696, 914-922.

Wang, Z., Ying, Y., Li, L., Xu, T., Wu, Y., Guo, X., Wang, F., Shen, H., Wen, Y., Yang, H., 2017. Appl. Surf. Sci. 396, 832-840.

Wightman, R.M., May, L.J., Michael, A.C., 1988. Anal. Chem. 60, 769A.

Xiao, X., Zhou, B., Liang, T., Tang, H., Zhang, Y., Xie, Q., Yao, S., 2011. Electrochim. Acta 56, 10055-10063.

XX, K., AP, K., SA, J., 2003. Macromolecules. 36, 8992-8999.

Yan, X., Gu, Y., Li, C., Tang, L., Zheng, B., Li, Y., Zhang, Z., Yang, M., 2016. Biosens. Bioelectron. 77, 1032.

Yao, L., Zhang, S., Wang, R., Li, W., Shen, F., Yang, B., Ma, Y., 2014. Angew. Makromol. Chem. 53, 2119.

Yeh, H.C., Yeh, S.J., Chen, C.T., 2003. Chem. Commun. 9, 2632.

Zhang, G., Wen, Y., Li, Y., Xu, J., Guo, C., Lu, B., Zhu, D., 2013a. J. Fluoresc. 23, 1053-1063.

Zhang, L., Yang, D., Wang, L., 2013b. Electrochim. Acta 111, 9-17.

Zhang, W., Chen, P., Zhou, L., Qin, Z., Gao, K., Yao, J., Li, C., Wang, P., 2017. Biosens. Bioelectron. 92, 523-528.

Zhang, X., Zhao, Z., Lou, X., Li, J., Hui, G., 2016. Journal of Food Measurement & Characterization, 1-8.

Zhou, J., Qiu, X., Su, K., Xu, G., Wang, P., 2016. Sensors and Actuators B: Chemical 235, 170-178.

Zou, L., Tian, Y., Zhang, X., Fang, J., Hu, N., Wang, P., 2017. Sensors and Actuators B: Chemical 238, 1173-1180.

Figure Captions

Fig. 1. (a) FT-IR spectra of PTBFN (A) and (B) (b) UV-vis spectra of PTBFN (A) and poly(PTBFN) (B) (c) SEM images of poly(PTBFN) (d) EIS curves of bare GCE (A)

and poly(PTBFN)/GCE (B)

Scheme 1. Illustration of fabrication process of the sensor and DA electrocatalytic oxidation.

Fig. 2. (a) CVs of the bare GCE (A) and the poly(PTBFN)/GCE (B and C) in 0.1M PBS (pH = 6) in the presence (A and B) and absence (C) of 300 μM DA, respectively. Scan rate: 0.10 V s^{-1}. (b) Chronoamperograms recorded for the poly(PTBFN)/GCE in absence (I_L) and presence (I_C) of 300 μM DA. Inset: the relation of I_C/I_L versus $t^{1/2}$.

Fig. 3. (a) CVs of 300 μM DA in 0.1M PBS at the poly(PTBFN)/GCE with pH (3.0–9.0). Scan rate: 0.10 V s^{-1}. (b) Plots of cathodic peak potentials and the inset of peak currents versus pH values.

Fig. 4. (a) CVs of 300 μM DA in 0.1M PBS (pH = 6) at poly(PTBFN)/GCE with different scan rates (30, 50, 80, 110, 140, 170, 200, 230, 260, 290, 320, 350, 380, 410, 440, 470, 500 mV s^{-1}). (b) The dependence of the corresponding peak current against square root of scan rates.

Fig. 5. (a) DPVs recorded by adding of DA at concentrations (5, 10, 50, 100, 500, 1000, 5000, 10000, 50000, 100000, 200000, 300000 and 350000nM) in 0.1M PBS (pH = 6) utilizing poly(PTBFN)/GCE. (b) The linear relationship between logarithm of peak current and dopamine concentration.

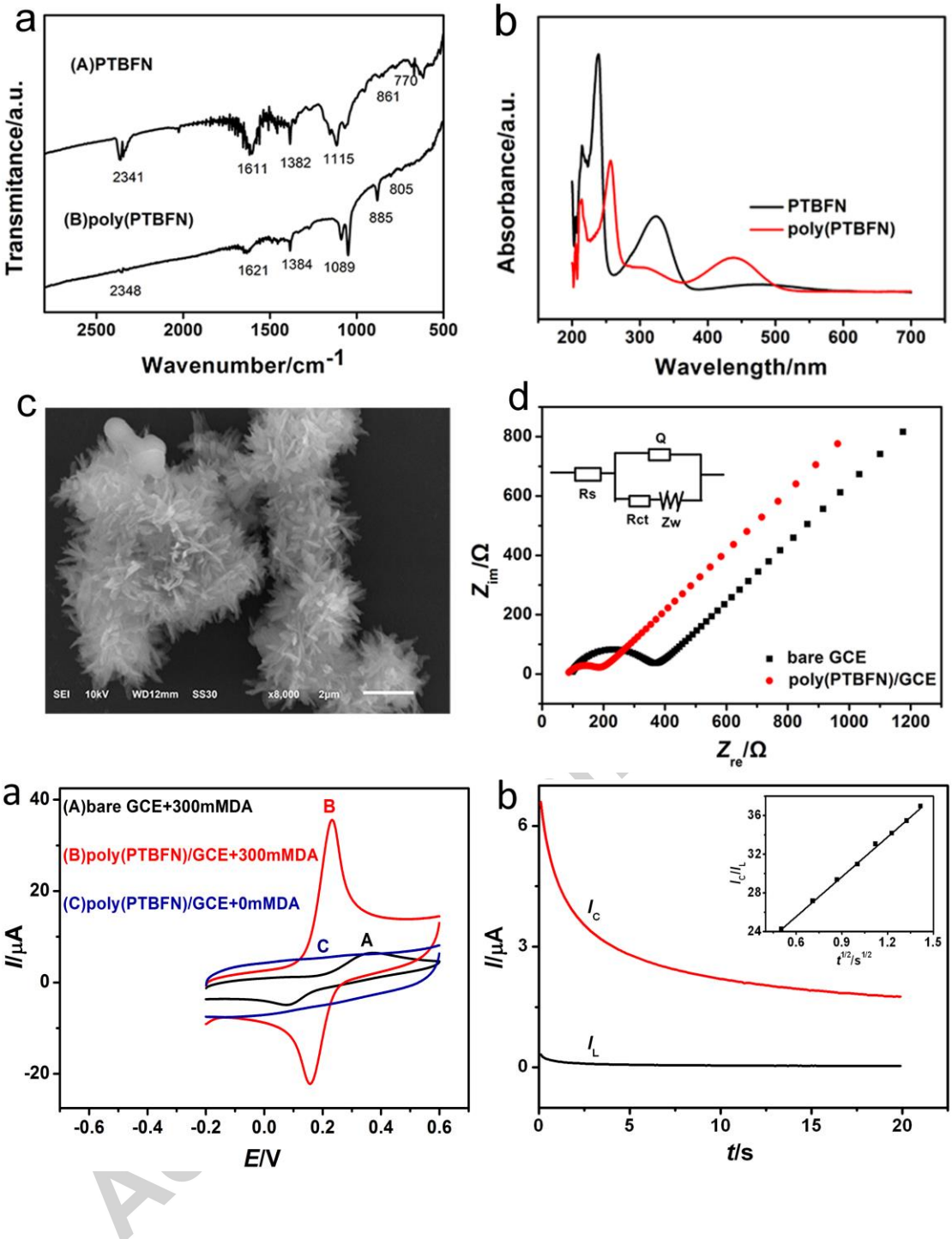
a
(A)PTBFN
770
861
2341
1611
1382
1115
(B)poly(PTBFN)
805
885
1621
1384
1089
2348
Transmitance/a.u.
2500
2000
1500
1000
500
Wavenumber/cm-1
b
Absorbance/a.u.
PTBFN
poly(PTBFN)
200
300
400
500
600
700
Wavelength/nm
c
SEI 10kV WD12mm SS30 x8,000 2μm
d
Q
Rs
Rct
Zw
Zim/Ω
bare GCE
poly(PTBFN)/GCE
Zre/Ω
a
(A)bare GCE+300mMDA
(B)poly(PTBFN)/GCE+300mMDA
(C)poly(PTBFN)/GCE+0mMDA
B
C
A
I/μA
E/V
b
Ic
IL
I/μA
t/s
Ic/IL
t1/2/s1/2

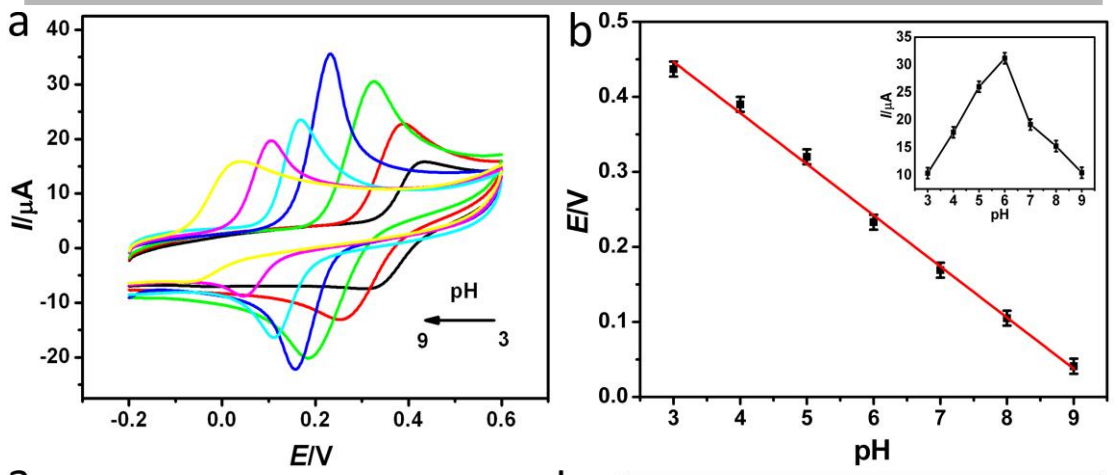

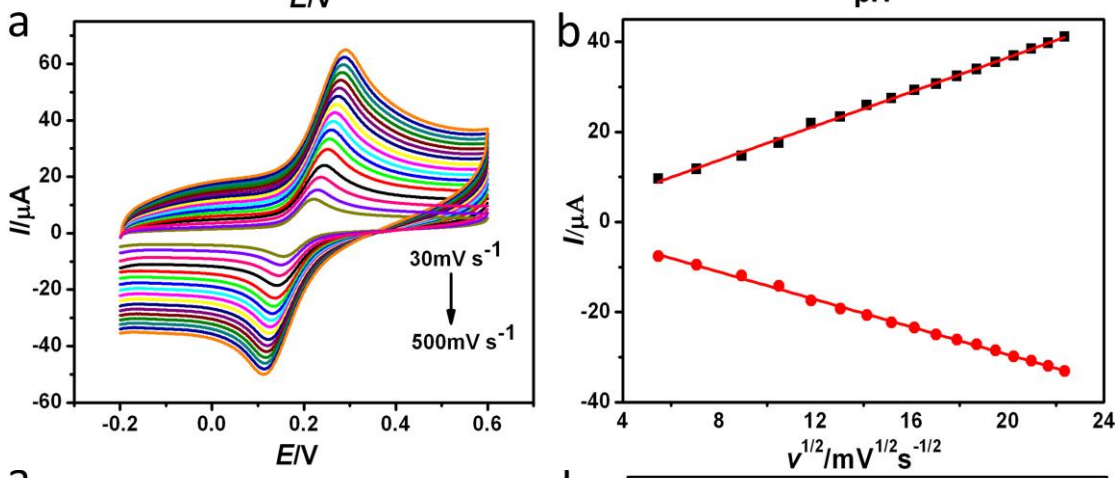

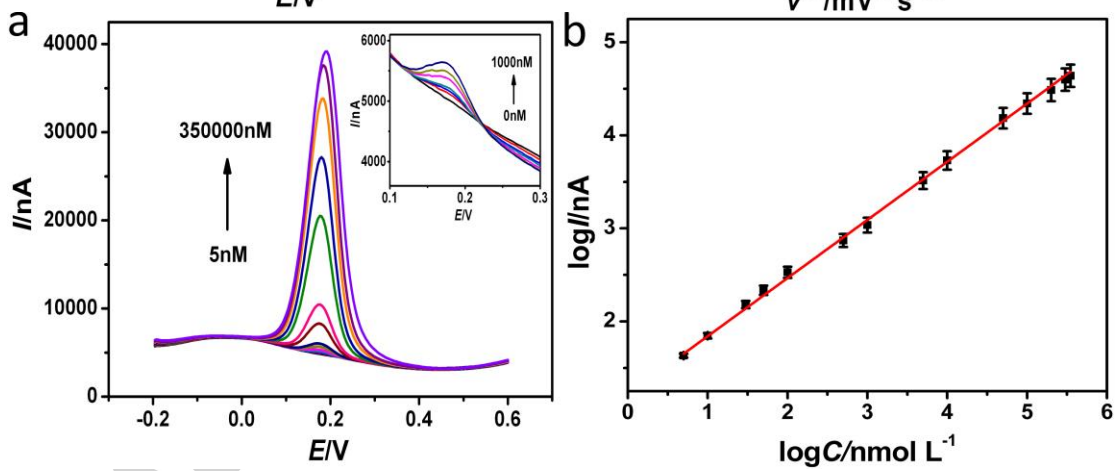

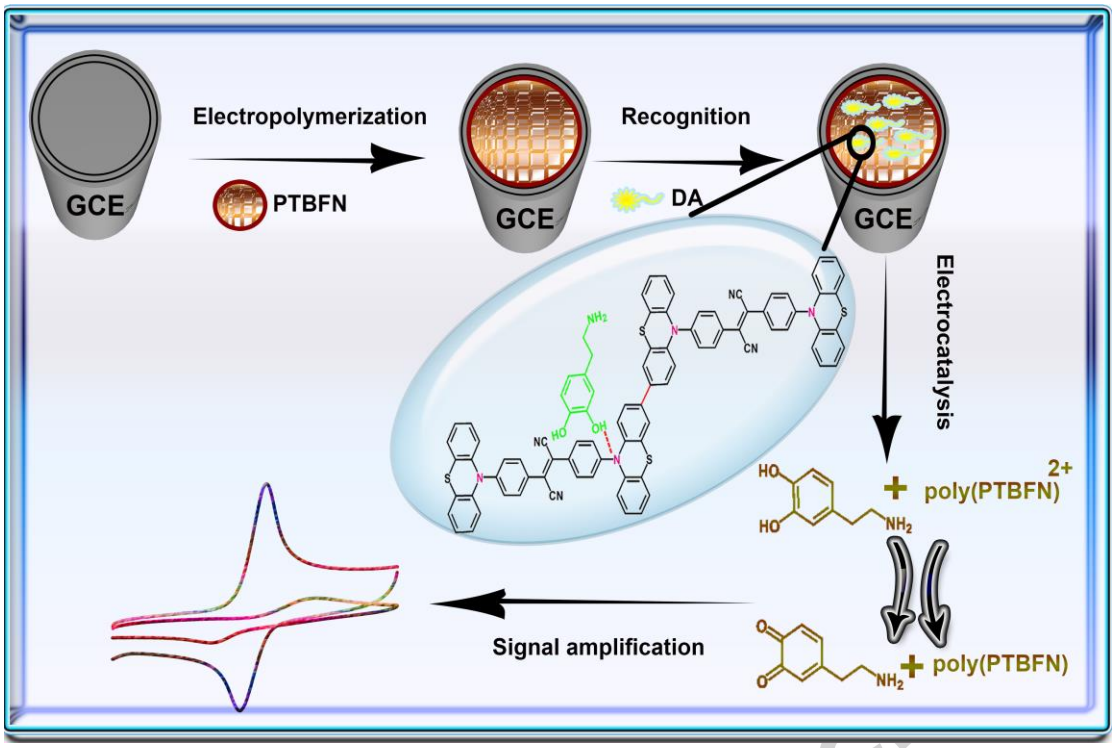

Highlights

(1) D–A structure biosensor is ultrasensitive due to amplification by the collective current signal.

(2) Bioaffinity recognition of phenothiazine–based assays.

(3) Future prospects to improve the biosensors are provided.